Available online at www.sciencedirect.com

CERAMICS INTERNATIONAL

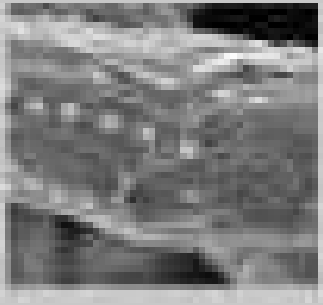

Submit Your Paper

Supports Open Access (https://www.elsevier.com/journals/ceramics-international/0272-8842/open-access-options)

View Articles (https://www.sciencedirect.com/science/journal/02728842)

Guide for Authors

Abstracting/ Indexing (http://www.elsevier.com/journals/ceramics-international/0272-8842/abstracting-indexing)

Track Your Paper

Order Journal (https://www.elsevier.com/journals/institutional/ceramics-international/0272-8842)

Journal Metrics

› CiteScore: **6.1**

Impact Factor: **3.830**

5-Year Impact Factor: **3.513**

Source Normalized Impact per Paper (SNIP): **1.310**

SCImago Journal Rank (SJR): **0.891**

› View More on Journal Insights

Your Research Data

› Share your research data (https://www.elsevier.com/authors/author-resources/research-data)

Related Links

› Author Stats

› Researcher Academy

› Author Resources (https://www.elsevier.com/authors/author-resources)

› Try out personalized alert features

Ceramics International - Editorial Board

General Editor

P. Vincenzini

World Academy of Ceramics, National Research Council, Faenza, Italy

Editors-in-Chief

R.K. Bordia

Clemson University, Clemson, South Carolina, United States

Z.Y. Fu

Ministry of Education of the Peoples Republic of China Changjiang Scholar Program, Wuhan, China

T. Ohji

National Institute of Advanced Industrial Science and Technology Advanced Manufacturing Research Institute, Tsukuba, Japan

V.C. Pandolfelli (https://www.journals.elsevier.com:443/ceramics-international/editorial-board/vc-pandolfelli)
Federal University of Sao Carlos Department of Materials Engineering, SAO CARLOS, Brazil

R. Riedel

Technical University of Darmstadt Department of Materials and Earth Sciences, Darmstadt, Germany

Associate Editor

Z.J. Yu

Xiamen University, Xiamen, China

Editorial Board

National Institute for Materials Science, 305-0044, Tsukuba-Shi, Japan

Z.J. Shen
Stockholm University Department of Materials and Environmental Chemistry, S-106 91, Stockholm, Sweden

W. Sigmund
University of Florida Department of Materials Science and Engineering, 225 Rhines Hall, P.O. Box 116400, Gainesville, Florida, 32611-6400, United States

M. Singh
NASA John H Glenn Research Center, MS 106-5 Ceramic Branch, Cleveland, Ohio, OH 44135-3191, United States

G. Srinivasan
Oakland University, Rochester, Michigan, 48309-4401, United States

D. Suvorov
Jozef Stefan Institute, 1000, Ljubljana, Slovenia

T. Troczynski
The University of British Columbia, Vancouver, V6T 1Z4, British Columbia, Canada

W.H. Tuan
National Taiwan University Department of Materials and Science Engineering, No. 1, Sec. 4, Roosevelt Road, 10617, Taipei, Taiwan

A. Vinu
Newcastle University, NE1 7RU, Newcastle, United Kingdom

M. Wang
Tongji University College of Design and Innovation, Shanghai, China

S. Yin
Tohoku University, 2-1-1 Katahira, Aoba-ku, 980-8577, Sendai, Japan

N. Zhou
Henan University of Technology, Luoyang, China

Y. Zhou
Chinese Academy of Sciences, China

Y. Zhou
Harbin Institute of Technology Institute of Advanced Ceramics, 92 West Dazhi Street, Nan'gang District, 150001, Harbin, China

Ceramics International

Readers
View Articles

Volume 46, Issue 10, Part A

Pages 14317-15724 (July 2020)

Previous vol/issue Next vol/issue

Reviews

Original Articles

Research article ○ Abstract only

Modelling and experimental investigation of pore-like flaw-strength response in structural ceramics

Anzhe Wang, Ping Hu, Xinyuan Zhao, Zhizhi Wang, ... Yongzheng Wang

Pages 14431-14438

Purchase PDF Article preview

Research article ○ Abstract only

Thermal/vibration joint experimental investigation on lightweight ceramic insulating material for hypersonic vehicles in extremely high-temperature environment up to 1500 °C

Dafang Wu, Lujin Lin, Haoyuan Ren

Pages 14439-14447

Purchase PDF Article preview

Research article ○ Abstract only

Synthesis, characterization and in vitro evaluation of zinc and strontium binary doped hydroxyapatite for biomedical application

Ihsan Ullah, Muhammad Ali Siddiqui, Sharafadeen Kunle Kolawole, Hui Liu, ... Ke Yang

Pages 14448-14459

Purchase PDF Article preview

Research article ○ Abstract only

Phase transformations and changes in the dielectric properties of nanostructured perovskite-like LBZ composites as a result of thermal annealing

Maxim Zdorovets, Artem Kozlovskiy, Alexander Arbuz, Darya Tishkevich, ... Alexey Trukhanov

Pages 14460-14468

Purchase PDF Article preview

Research article ○ Abstract only

Synthesis of W_2B_5 powders by the reaction between WO_3 and amorphous B in NaCl/KCl flux

Bing Dai, Xiang Ding, Xiangong Deng, Jianhua Zhu, Songlin Ran

Pages 14469-14473

Purchase PDF Article preview

Research article ○ Abstract only

Fabrication and properties of mullite thermal insulation materials with in-situ synthesized mullite hollow whiskers

Hao Liu, Xun Xiong, Minghao Li, Zhoufu Wang, ... Lin Yuan

Pages 14474-14480

Purchase PDF Article preview

Research article ○ Abstract only

Structural and magnetic features of Ce doped Co-Cu-Zn spinel nanoferrites prepared using sol gel self-ignition method

Sabih Qamar, Majid Niaz Akhtar, Khalid Mujasam Batoo, Emad H. Raslan

Pages 14481-14487

Purchase PDF Article preview

Research article ○ Abstract only

Bubble-sheet-like $Ni_{0.85}Co_{2.15}V_2O_8$ nanosheets for high-rate lithium storage

Magnetic complex permeability (imaginary part) dependence on the microstructure of a Cu-doped Ni–Zn-polycrystalline sintered ferrite
A. Barba, C. Clausell, J.C. Jarque, L. Nuño
Pages 14558-14566

Purchase PDF Article preview

Research article ○ Abstract only
Photocurrent and dielectric/ferroelectric properties of $KNbO_3$–$BaFeO_{3-\delta}$ ferroelectric semiconductors
Fei Han, Yujie Zhang, Changlai Yuan, Xiao Liu, ... Guanghui Rao
Pages 14567-14572

Purchase PDF Article preview

Research article ○ Abstract only
Synthesis of hollow TiO_2 nanobox with enhanced electrorheological activity
Changhao Li, Kai He, Weijian Sun, Baoxiang Wang, ... Kezheng Chen
Pages 14573-14582

Purchase PDF Article preview

Research article ○ Abstract only
Formation mechanism of stereolithography of Si_3N_4 slurry using silane coupling agent as modifier and dispersant
Yao Liu, Lijin Cheng, Hao Li, Qing Li, ... Shaojun Liu
Pages 14583-14590

Purchase PDF Article preview

Research article ○ Abstract only
Innovative design and fabrication of generation IV nuclear fuel embedded with carbon nanotube
P.T. Rao, Jyoti Prakash, Rajath Alexander, Amit Kaushal, ... Kinshuk Dasgupta
Pages 14591-14596

Purchase PDF Article preview

Research article ○ Abstract only
Morphological regulation and simulation of β-Sialon and its effect on thermo-mechanical properties of Al_2O_3-C refractories
Chaofan Yin, Xiangcheng Li, Pingan Chen, Yingli Zhu, Boquan Zhu
Pages 14597-14604

Purchase PDF Article preview

Research article ○ Abstract only
Dip-coated V doped ZnO thin films: Dielectric and magnetic properties
Zohra Nazir Kayani, Hina Nazli, Sania Kousar, Saira Riaz, Shahzad Naseem
Pages 14605-14612

Purchase PDF Article preview

Research article ○ Abstract only
Material removal behaviour in axial ultrasonic assisted scratching of Zerodur and ULE with a Vickers indenter
Guoyan Sun, Feng Shi, Qingliang Zhao, Zhen Ma, Donglai Yang
Pages 14613-14624

Purchase PDF Article preview

Research article ○ Abstract only

Densification and oxidation behavior of spark plasma sintered Hafnium Diboride-Hafnium Carbide composite

Catalina Young, Cheng Zhang, Archana Loganathan, Pranjal Nautiyal, ... Arvind Agarwal

Pages 14625-14631

Purchase PDF Article preview

Research article ○ Abstract only

Unprecedented oxidation resistance at 900 °C of Mo–Si–B composite with addition of ZrB_2

Juan Wang, Bin Li, Rui Li, Xuan Chen, ... Guojun Zhang

Pages 14632-14639

Purchase PDF Article preview

Research article ○ Abstract only

Capacitive property studies of electrochemically synthesized Co_3O_4 and Mn_3O_4 on inexpensive stainless steel current collector for supercapacitor application

Nagesh Maile, S.K. Shinde, S.S. Patil, D.-Y. Kim, ... V.J. Fulari

Pages 14640-14649

Purchase PDF Article preview

Research article ○ Abstract only

Ag NPs modified plasmonic Z-scheme photocatalyst $Bi_4Ti_3O_{12}/Ag/Ag_3PO_4$ with improved performance for pollutants removal under visible light irradiation

Chuanwei Lin, Jianqing Ma, Futao Yi, Huining Zhang, ... Kefeng Zhang

Pages 14650-14661

Purchase PDF Article preview

Research article *Open access*

Statistical study of compressive creep parameters of an alumina spinel refractory

Soheil Samadi, Shengli Jin, Dietmar Gruber, Harald Harmuth, Stefan Schachner

Pages 14662-14668

Download PDF Article preview

Research article ○ Abstract only

Investigation of grain growth and magnetic properties of low-sintered LiZnTi ferrite-ceramic

Fang Xu, Xiaolei Shi, Yulong Liao, Jie Li, Jianbo Hu

Pages 14669-14673

Purchase PDF Article preview

Research article ○ Abstract only

Inversion degree, morphology and colorimetric parameters of cobalt aluminate nanopigments depending on reductant type in solution combustion synthesis

Tetiana Tatarchuk, Alexander Shyichuk, Jan Lamkiewicz, Joanna Kowalik

Pages 14674-14685

Purchase PDF Article preview

Research article ○ Abstract only

Effects of BN layer on photoelectric properties and stability of flexible Al/Cu/ZnO multilayer thin film

Research article ○ Abstract only

Characterization and ablation resistance of ZrB_2-xSiC gradient coatings deposited with HPPS

Yixin Bai, Quansheng Wang, Zhuang Ma, Yanbo Liu, ... Shijie Sun

Pages 14756-14766

Purchase PDF Article preview

Research article ○ Abstract only

Ti_2AlC bulk ceramics produced by gelcasting and Al-rich pressureless sintering

Zhanchong Zhao, Huayan Liu, Xianhui Li, Yan Zhuang, ... Qingzhi Yan

Pages 14767-14775

Purchase PDF Article preview

Research article ○ Abstract only

Synthesis and characterisation of nanocrystalline CuO–Fe_2O_3/GDC anode powders for solid oxide fuel cells

Mohammadmehdi Choolaei, Timothy Bull, Tomas Ramirez Reina, Bahman Amini Horri

Pages 14776-14786

Purchase PDF Article preview

Research article ○ Abstract only

On the simulation of spark plasma sintered TiB_2 ultra high temperature ceramics: A numerical approach

Mehdi Fattahi, Meysam Najafi Ershadi, Mohammad Vajdi, Farhad Sadegh Moghanlou, ... Mehdi Shahedi Asl

Pages 14787-14795

Purchase PDF Article preview

Research article ○ Abstract only

A functionalized Sm/Sr doped TiO_2 nanotube array on titanium implant enables exceptional bone-implant integration and also self-antibacterial activity

Xuejiao Zhang, Yong Huang, Bingbing Wang, Xiaotong Chang, ... Xiaojun Zhang

Pages 14796-14807

Purchase PDF Article preview

Research article ○ Abstract only

In-situ synthesis and properties of porous cordierite ceramics with adjustable pore structure

Hao Li, Cuiwei Li, Linghao Wu, Han Wang, ... Chang-An Wang

Pages 14808-14815

Purchase PDF Article preview

Research article ○ Abstract only

Enhanced energy storage capability of (1-x)$Na_{0.5}Bi_{0.5}TiO_3$-x$Sr_{0.7}Bi_{0.2}TiO_3$ free-lead relaxor ferroelectric thin films

Jie Ding, Zhongbin Pan, Peixu Chen, Di Hu, ... Jiwei Zhai

Pages 14816-14821

Purchase PDF Article preview

Research article ○ Abstract only

Ratio effect of salt fluxes on structure, dielectric and magnetic properties of La,Mn-doped $PbBi_2Nb_2O_9$ Aurivillius phase

Tio Putra Wendari, Syukri Arief, Nandang Mufti, Jacob Baas, ... Zulhadjri

Pages 14822-14827

Purchase PDF Article preview

Research article ○ Abstract only

Electric-potential-induced uniformity in graphene oxide deposition on porous alumina substrates

Hyeonho Cho, Seok-min Kim, Hong Liang, Sunghan Kim

Pages 14828-14839

Purchase PDF Article preview

Research article ○ Abstract only

Tuning the ratio of Al_2O_3 to $LiAlO_2$ in the composite coating layer for high performance $LiNi_{0.5}Mn_{1.5}O_4$ materials

Yang Shu, Yin Xie, Wenchao Yan, Su Meng, ... Lan Xiang

Pages 14840-14846

Purchase PDF Article preview

Research article ○ Abstract only

Mechanism of enhanced magnetization in $CoFe_2O_4/La_{0.7}Sr_{0.3}MnO_3$ composites with different mass ratios

Xian Zhang, Xucai Kan, Min Wang, Rui Rao, ... Yongqing Ma

Pages 14847-14856

Purchase PDF Article preview

Research article ○ Abstract only

Ni-doped $LiFePO_4$/C as high-performance cathode composites for Li-ion batteries

Yuan Liu, Yi-Jing Gu, Gui-Yang Luo, Zi-Liang Chen, ... Jun-Qi Li

Pages 14857-14863

Purchase PDF Article preview

Research article ○ Abstract only

Stabilization of the γ-Ag_2WO_4 metastable pure phase by coprecipitation method using polyvinylpyrrolidone as surfactant: Photocatalytic property

N.F. Andrade Neto, J.M.P. Silva, R.L. Tranquilin, E. Longo, ... F.V. Motta

Pages 14864-14871

Purchase PDF Article preview

Research article ○ Abstract only

Fabrication of a leaf-like superhydrophobic CuO coating on 6061Al with good self-cleaning, mechanical and chemical stability

Zhexin Lv, Sirong Yu, Kaixing Song, Xue Zhou, Xiaoli Yin

Pages 14872-14883

Purchase PDF Article preview

Research article ○ Abstract only

Research on thermal shock resistance of porous refractory material by strain-life fatigue approach

Yunjian Luo, Huazhi Gu, Meijie Zhang, Ao Huang, ... Peizhong Yan

Pages 14884-14893

Purchase PDF Article preview

Research article ○ Abstract only

A sustainable reaction process for phase pure $LiFeSi_2O_6$ with goethite as an iron source

Research article ○ Abstract only

Study on solidification properties of chemically bonded phosphate ceramics for cesium radionuclides

Yan Tao, Lai Zhenyu, Ren Chunrong, Wang Yuanyuan, ... Lv Shuzhen

Pages 14964-14971

Purchase PDF Article preview

Research article ○ Abstract only

Enhanced photocatalytic degradation, micro-structural evolution and optical performance of SZ/TiO_2 nano-composite materials

F. Alharbi, I.H. Mejri, W. Hzez, K. Omri

Pages 14972-14977

Purchase PDF Article preview

Research article ○ Abstract only

Manipulation of Curie temperature and ferroelectric polarization for large electrocaloric strength in $BaTiO_3$-based ceramics

Zhibin Lv, Jie Wei, Tiantian Yang, Zehao Sun, Zhuo Xu

Pages 14978-14984

Purchase PDF Article preview

Research article ○ Abstract only

RGO-supported core-shell SiO_2@SiO_2/carbon microsphere with adjustable microwave absorption properties

Xiaomeng Fan, Ruizhe Yuan, Xin Li, Hailong Xu, ... Laifei Cheng

Pages 14985-14993

Purchase PDF Article preview

Research article ○ Abstract only

Achieving a fine balance in mechanical properties and thermoelectric performance in commercial Bi_2Te_3 materials

Yu-Ke Zhu, Peng Wu, Jun Guo, Yunxuan Zhou, ... Jing Feng

Pages 14994-15002

Purchase PDF Article preview

Research article ○ Abstract only

Preparation and synthesis mechanism of ytterbium monosilicate nano-powders by a cocurrent coprecipitation method

Nan-nan Wu, Ya-lei Wang, Ru-tie Liu, Huai-fei Liu, ... Xiang Xiong

Pages 15003-15012

Purchase PDF Article preview

Research article ○ Abstract only

Improved thermoelectric performance of Al and Sn doped ZnO nano particles by the engineering of secondary phases

Jolly Jacob, U. Rehman, K. Mahmood, A. Ali, ... Fouzia Ashraf

Pages 15013-15017

Purchase PDF Article preview

Research article ○ Abstract only

Effects of microwave-assisted hydrothermal treatment and beta particles irradiation on the thermoluminescence and optically stimulated luminescence of $SrMoO_4$ powders

Roseli Künzel, Nancy K. Umisedo, Emico Okuno, Elisabeth Mateus Yoshimura, Ana Paula de Azevedo Marques

Pages 15018-15026

Purchase PDF Article preview

Research article ○ Abstract only

Radiation shielding properties of PNCKM bioactive glasses at nuclear medicine energies

Amani Alalawi, M.S. Al-Buriahi, Y.S. Rammah

Pages 15027-15033

Purchase PDF Article preview

Research article ○ Abstract only

Synthesis and characterization of CeO_2/rGO nanoflakes as electrode material for capacitive deionization technology

Ayman Yousef, Abdullah M. Al-Enizi, Ibrahim M.A. Mohamed, M.M. El-Halwany, ... Robert M. Brooks

Pages 15034-15043

Purchase PDF Article preview

Research article ○ Abstract only

Microwave sintering of a nanostructured low-level additive ZnO-based varistor

Rodolfo F.K. Gunnewiek, Claudia P.F. Perdomo, Igor C. Cancellieri, André L.F. Cardoso, Ruth H.G.A. Kiminami

Pages 15044-15053

Purchase PDF Article preview

Research article ○ Abstract only

Luminescence of Cr^{3+}/Yb^{3+} co-doped oxyfluoride silicate glasses for crystalline silicon solar cell down-conversion devices

Wenbin Fu, Chaomin Zhang, Zhangwen Li, Jinan Xia, Yunxia Ping

Pages 15054-15060

Purchase PDF Article preview

Research article ○ Abstract only

Superior ferroelectric photovoltaic properties in Fe -modified (Pb,La) $(Zr,Ti)O_3$ thin film by improving the remnant polarization and reducing the band gap

Guang Chen, Ying Zhang, Qingfeng Zhang, Yinmei Lu, Yunbin He

Pages 15061-15065

Purchase PDF Article preview

Research article ○ Abstract only

Effect of Mo on tribological behaviors of atmospheric plasma sprayed Al_2O_3-13%TiO_2/Mo coatings under boundary lubrication condition

Chao Zhang, Bo Huang, Jinyong Xu, Wenjian Cao, ... Shuo Yin

Pages 15066-15075

Purchase PDF Article preview

Research article ○ Abstract only

Enhanced electrical properties of ZnO varistor ceramics by spark plasma sintering: Role of annealing

Jie Liang, Xuetong Zhao, Jianjie Sun, Lulu Ren, ... Weiwei Li

Pages 15076-15083

Purchase PDF Article preview

Research article ○ Abstract only

Atmospheric pressure chemical vapor infiltration of a titanium carbide interphase coating on carbon fiber

Chris Monteleone, Shannon Poges, Kenneth Petroski, Peter Kerns, ... Steven L. Suib

Pages 15084-15091

Purchase PDF Article preview

Research article ○ Abstract only

Processing of Zn-Substituted calcium silicate layers on Y-Tzp bioceramics by dip coating

Yesica L. Bruni, Thomas P. Puleston, María P. Albano

Pages 15092-15103

Purchase PDF Article preview

Research article ○ Abstract only

Elastic and thermodynamic properties of high entropy carbide (HfTaZrTi)C and (HfTaZrNb)C from ab initio investigation

Shan Jiang, Lin Shao, Tou-Wen Fan, Jia-Ming Duan, ... Bi-Yu Tang

Pages 15104-15112

Purchase PDF Article preview

Research article ○ Abstract only

Effects of heat treatment on the crystallization behavior, microstructure and thermal properties of a complex Li_2O-SiO_2 glass system

Yangshan Sun, Liyun Ma, Pingping Wang, Zhenkun Ke, ... Tianhe Wang

Pages 15113-15121

Purchase PDF Article preview

Research article ○ Abstract only

Mechanism and feasibility of ultrasonic-assisted milling to improve the machined surface quality of 2D C_f/SiC composites

Jie Chen, Weiwei Ming, Qinglong An, Ming Chen

Pages 15122-15136

Purchase PDF Article preview

Research article ○ Abstract only

Mechanical characterisation and machining evaluation of ceramic cutting tools functionally graded with six layers

M. Bertolete, P.A. Barbosa, W. de Rossi, C. Fredericci, I.F. Machado

Pages 15137-15145

Purchase PDF Article preview

Research article ○ Abstract only

Synthesis of NiAl-WC composite by the thermal explosion of elemental powders

Shu-Rong Yan, Majid Zarezadeh Mehrizi, Loke Kok Foong

Pages 15146-15151

Purchase PDF Article preview

Research article ○ Abstract only

Aerosol assisted chemical vapour deposition of nanostructured ZnO thin films for NO_2 and ethanol monitoring

Jian Ding, Shuqun Chen, Ning Han, Yi Shi, ... Jinshu Wang

Pages 15152-15158

Purchase PDF Article preview

Research article ○ Abstract only

Porous Al_2O_3 ceramics with spontaneously formed pores and enhanced strength prepared by indirect selective laser sintering combined with reaction bonding

Ye Dong, Hongyi Jiang, Annan Chen, Ting Yang, ... Dong Xu

Pages 15159-15166

Purchase PDF Article preview

Research article ○ Abstract only

Precursor infiltration and pyrolysis cycle-dependent mechanical and microwave absorption performances of continuous carbon fibers-reinforced boron-containing phenolic resins for low-density carbon-carbon composites

Yu Sun, Yuguo Sun

Pages 15167-15175

Purchase PDF Article preview

Research article ○ Abstract only

Carbon microsphere-templated synthesis of $ZnCo_2O_4$ hollow spheres functionalized with Ag nanoparticles for sub-ppm-level acetone gas detection

Dongzhi Zhang, Yingbo Jin, Haonan Chen, Yuwei Luo, Yong Zhang

Pages 15176-15182

Purchase PDF Article preview

Research article ○ Abstract only

Roughness and bearing analysis of ZnO nanorods

S. Kaya, O. Ozturk, L. Arda

Pages 15183-15196

Purchase PDF Article preview

Research article ○ Abstract only

Novel unidirectional porous carbon/carbon composites prepared by a special designed space holder method

Jiangang Jia, Shunwei Liu, Tingxi Xia, Bo Zhang, ... Genshun Ji

Pages 15197-15205

Purchase PDF Article preview

Research article ○ Abstract only

$(Ba_xMg_{1-x})(Ti_{0.95}Sn_{0.05})O_3$ (x = 0.025, 0.05, 0.075 and 0.1) solid solutions as effective Ku-band (12.4–18 GHz) shielders

Jasdeep Singh, Shalini Bahel

Pages 15206-15213

Purchase PDF Article preview

ISSN: 0272-8842

Previous vol/issue

Next vol/issue

Ceramics International 46 (2020) 14822–14827

Contents lists available at ScienceDirect

Ceramics International

journal homepage: www.elsevier.com/locate/ceramint

Ratio effect of salt fluxes on structure, dielectric and magnetic properties of La,Mn-doped $PbBi_2Nb_2O_9$ Aurivillius phase

Tio Putra Wendari[a], Syukri Arief[a], Nandang Mufti[b], Jacob Baas[c], Graeme R. Blake[c], Zulhadjri[a,*]

[a] Department of Chemistry, Faculty of Mathematics and Natural Sciences, Universitas Andalas, Kampus Limau Manis, Padang, 25163, Indonesia
[b] Department of Physics, Faculty of Mathematics and Natural Sciences, Universitas Negeri Malang, Jl. Semarang 5, Malang, 65145, Indonesia
[c] Zernike Institute for Advanced Materials, University of Groningen, Nijenborgh 4, 9747, AG Groningen, the Netherlands

ARTICLE INFO

Keywords:
Aurivillius phase
Molten salt method
Ferroelectric behavior
Double-exchange interaction

ABSTRACT

The double-layer Aurivillius phase $Pb_{0.4}Bi_{2.1}La_{0.5}Nb_{1.7}Mn_{0.3}O_9$ was synthesized by a molten salt method using a K_2SO_4/Na_2SO_4 flux. The effect on the crystal structure, morphology, dielectric and magnetic properties of varying the molar ratio of the oxide precursors to salt flux was investigated. Single-phase products with an orthorhombic structure were obtained for oxide to salt ratios of between 1:5 and 1:9, whereas for lower concentrations of salt a pyrochlore impurity phase is found in the products. SEM showed anisotropic plate-like grains, the size of which increases for larger salt ratios. An investigation of the magnetic properties showed the presence of mixed Mn^{3+} and Mn^{4+}; the unit cell volume of the single-phase products decreases as the proportion of salt increases, which implies a higher proportion of smaller Mn^{4+} cations. This can be explained by the oxide ion donating properties (oxobasicity) of the molten salt mixture, which produces an oxidizing environment during synthesis. The best dielectric properties are obtained for an oxide to salt ratio of 1:7, exhibiting relaxor ferroelectric behavior. This is also the ratio at which the most pronounced ferromagnetic properties are observed, resulting from double-exchange interactions between Mn^{3+} and Mn^{4+}, the proportions of which are approximately equal. $Pb_{0.4}Bi_{2.1}La_{0.5}Nb_{1.7}Mn_{0.3}O_9$ synthesized under these conditions thus exhibits optimal multiferroic properties.

1. Introduction

Ferroelectric materials belonging to the Aurivillius family have attracted much attention due to their high dielectric constants, large remanent polarization, low coercive fields, and high Curie temperatures, material properties that have potential use in random access memory (RAM) [1,2]. The Aurivillius structure is constructed by alternating perovskite blocks and bismuth oxide layers and can be represented by the general formula $(Bi_2O_2)^{2+}(A_{m-1}B_mO_{3m+1})^{2-}$, where A is a mono-, di-, or trivalent cation with dodecahedral coordination, B is a transition metal cation with octahedral coordination, and m is the number of octahedral layers within the perovskite-like blocks [3,4].

The ferroelectric Aurivillius compound $PbBi_2Nb_2O_9$ ($m = 2$) adopts a non-centrosymmetric crystal structure with the $A2_1am$ space group, and exhibits a high Curie temperature (T_c = 557 °C) due to the $6s^2$ lone pair electrons associated with Pb^{2+} and Bi^{3+}, which induce a highly distorted structure [5,6]. Studies with the aim of improving the properties of Aurivillius compounds have been conducted for decades, and the focus in recent years has been especially on possible multiferroic properties. The substitution of a d^n (n ≠ 0) cation on the perovskite B-site can potentially induce a ferromagnetic ordering [2,7]. Besides, the substitution of d^n cations might also result in a distortion of the BO_6 octahedra due to the effect of different ionic radii on the B-site, thus enhancing the ferroelectric properties [8,9]. Furthermore, the substitution of lanthanide ions on the perovskite A-site is well known in Aurivillius phases to improve the dielectric and piezoelectric properties, reduce the electrical conductivity and dielectric loss, and possibly lead to relaxor-ferroelectric behavior [10,11]. Therefore, the simultaneous substitution of both La^{3+} and Mn^{3+} (d^4) ions can potentially result in multiferroic properties, which is beneficial for the application of non-volatile memory.

Aurivillius phases are usually prepared by solid-state synthesis. However, the synthesis of single-phase multiferroic Aurivillius samples is challenging because impurities tend to be formed due to the different character of the transition metal d-orbitals and the difference in ionic radii when partial substitutions are performed [12]. High-temperature

* Corresponding author. Department of Chemistry, Faculty of Mathematics and Natural Sciences, Universitas Andalas, Kampus Limau Manis, Padang, 25163, Indonesia.
E-mail address: zulhadjri@sci.unand.ac.id (Zulhadjri).

https://doi.org/10.1016/j.ceramint.2020.03.007
Received 10 January 2020; Received in revised form 29 February 2020; Accepted 1 March 2020
Available online 02 March 2020

synthesis often leads to the volatilization of Bi^{3+} which requires the addition of excess Bi_2O_3 to the precursor mixture [13]. In many cases synthesis using a molten salt method is superior; the use of salt fluxes as the reaction medium gives many advantages such as lower-temperature synthesis, fast ionic diffusion, and high reaction rates [14]. Molten sulfate and chloride salts have been widely applied to synthesize multiferroic Aurivillius phases [8,15,16]. The precise nature of the salt flux plays a crucial role in determining the compositional and grain homogeneity of the product, which in turn strongly affects the physical properties. However, many reports on the molten salt synthesis of Aurivillius phases only focus on the role of the salt flux in the growth mechanism. Thus, our research aim is to determine the best flux ratio for obtaining single-phase products and optimal multiferroic properties.

Recently, we have reported on the preparation of the La,Mn-doped $PbBi_2Nb_2O_9$ phase with chemical formula $Pb_{1-2x}Bi_{1.5+2x}La_{0.5}Nb_{2-x}Mn_xO_9$ using a K_2SO_4/Na_2SO_4 molten salt flux with a ratio of 1:7 oxide to salt [17]. A single-phase product was obtained for the maximum achievable Mn content of $Pb_{0.4}Bi_{2.1}La_{0.5}Nb_{1.7}Mn_{0.3}O_9$, which exhibits the best dielectric properties of this doping series and exhibit the pronounced ferromagnetic properties [18]. This compound is also interesting to explore because of the reduced lead content which represents a more environmentally friendly material compared to $PbBi_2Nb_2O_9$. Therefore, we continue our studies of this material by investigating the effect of the oxide to salt ratio on the purity, crystal structure, morphology, dielectric and magnetic properties. The molar ratio of oxide to salt was varied from 1:0 to 1:9.

2. Experimental procedures

The precursors PbO, Bi_2O_3, La_2O_3, Nb_2O_5, and Mn_2O_3 (Aldrich, ≥ 99.9%) were weighed in a stoichiometric ratio for the target formula $Pb_{0.4}Bi_{2.1}La_{0.5}Nb_{1.7}Mn_{0.3}O_9$ and mixed and ground in an agate mortar with added ethanol for 2 h. A 1:1 molar ratio of K_2SO_4/Na_2SO_4 salts was then added to the precursor mixture to give molar ratios of oxide to salt of 1:0, 1:3, 1:5, 1:7, and 1:9, denoted as samples PBLNM0, PBLNM3, PBLNM5, PBLNM7, and PBLNM9, respectively. The mixtures were successively calcined at 750 °C, 850 °C and 950 °C for 5 h each with a heating rate of 5 °C/min. After heating at each temperature, the powders were slowly cooled to room temperature and reground. The products were finally washed several times with hot distilled water to remove the sulfate salts and then dried at 110 °C for 5 h. The crystalline phases in the products were analyzed by X-ray diffraction (Shimadzu XRD 7000). The unit cells were refined by the Le Bail refinement technique using the RIETICA program. Scanning electron microscopy (FEI INSPECT S50) was used to observe the grain morphology. For dielectric measurements, the powder was pressed into pellets and sintered at 900 °C for 5 h. Silver conductive paste (Aldrich, 99%) was applied to both surfaces of the sintered pellet to form electrodes and heated at 110 °C for 2 h. The dielectric measurements were carried out using a precision LCR-meter (Agilent 4980A) with an amplitude of 1 V in the temperature range 30 to 500 °C at a frequency of 1 MHz. The magnetization was measured using a SQUID magnetometer (Quantum Design MPMS XL7) in the temperature range from 5 to 300 K under a magnetic field of 1 T. Magnetization as a function of applied field was measured from -5 T to 5 T at a temperature of 5 K.

3. Results and discussion

Fig. 1 shows XRD patterns of $Pb_{0.4}Bi_{2.1}La_{0.5}Nb_{1.7}Mn_{0.3}O_9$ synthesized using varying salt ratios. All the XRD patterns are indexed using the standard pattern of the double-layer Aurivillius phase $PbBi_2Nb_2O_9$, which has an orthorhombic structure with the $A2_1am$ space group (ICSD-95920). Single-phase products were obtained for PBLNM5, PBLNM7 and PBLNM9, while for PBLNM0 and PBLNM3 a pyrochlore impurity phase was detected. The formation of the pyrochlore phase might be caused by bismuth volatilization during high-temperature processing [15,19]. It is expected that the salt flux plays a crucial role as a reaction medium, enhancing the solubility of the oxide precursors, facilitating ion diffusion and suppressing Bi^{3+} volatilization. Moreover, the formation of single-phase $Pb_{0.4}Bi_{2.1}La_{0.5}Nb_{1.7}Mn_{0.3}O_9$ suggests that 0.5 moles of La^{3+} can be incorporated on the *A*-site of $PbBi_2Nb_2O_9$ and 0.3 moles of Mn^{3+} on the *B*-site, and that a minimum ratio of oxide to salt of 1:5 is required.

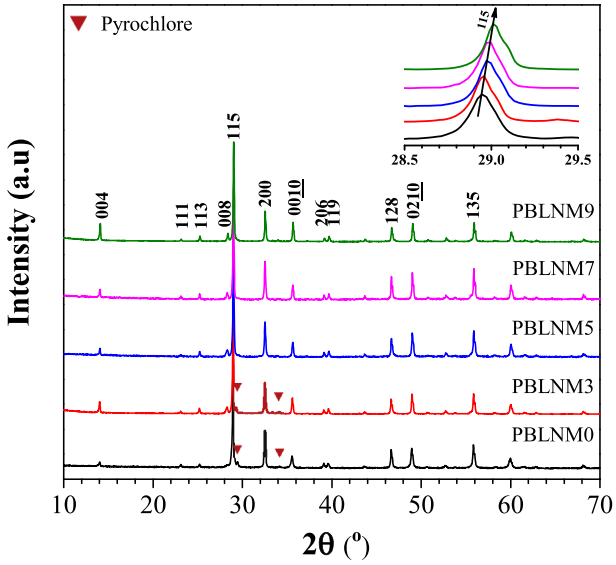

Fig. 1. XRD patterns of $Pb_{0.4}Bi_{2.1}La_{0.5}Nb_{1.7}Mn_{0.3}O_9$ powders prepared by the molten salt method with different oxide to salt ratios.

With increasing salt ratio, the full width at half maximum (FWHM) of the XRD peaks decreases, indicating an increase in crystallinity. The average crystallite size calculated using Scherrer's formula is approximately 48 nm, 56 nm, 65 nm, 67 nm and 69 nm for samples PBLNM0, PBLNM3, PBLNM5, PBLNM7, and PBLNM9, respectively. These results suggest that the salt flux accelerates grain growth during the heating process [20]. It is also observed (see the inset of Fig. 1) that the most intense diffraction peak (115) shifts to higher 2θ with increasing salt ratio, implying a decrease in lattice parameters and cell volume.

The effect of the salt ratio on the grain size and morphology of $Pb_{0.4}Bi_{2.1}La_{0.5}Nb_{1.7}Mn_{0.3}O_9$ was investigated using SEM as shown in Fig. 2. Anisotropic plate-like grains are observed for all samples, which is typical for Aurivillius phases. However, both the size and morphology are significantly affected by the salt ratio. The average grain size of PBLNM0 is approximately 1.0 μm with the highest degree of agglomeration. As the salt ratio increases, the average grain size increases to 1.6 μm, 1.8 μm, 2.3 μm, and 2.4 μm for PBLNM3, PBLNM5, PBLNM7, and PBLNM9, respectively. Moreover, a decrease in agglomeration is observed and the grain shape becomes more uniform. It is known that grain growth is accelerated when salt fluxes are used as the reaction medium, leading to larger grain sizes when the proportion of salt used is higher [21]. Furthermore, the flux diffuses between the grains and prevents the occurrence of agglomeration at higher salt ratios [20].

Refinement of the lattice parameters was carried out using the Le Bail method only for the single-phase products PBLNM5, PBLNM7 and PBLNM9, using the structural parameters of orthorhombic $PbBi_2Nb_2O_9$ with space group $A2_1am$ [22] as the initial model. The profile plots in Fig. 3 show good fits for all three samples and suggest that the products also adopt the non-centrosymmetric $A2_1am$ structure of the parent compound. The refined lattice parameters and unit cell volumes are given in Table 1. The *a* and *b* lattice parameters are essentially the same for the three samples, whereas the *c* lattice parameter significantly decreases as the salt ratio increases, leading to a decrease in cell volume. This implies a shrinkage of the BO_6 octahedra due to a shortening of the *B*–O bond lengths and could occur due to a varying proportion of

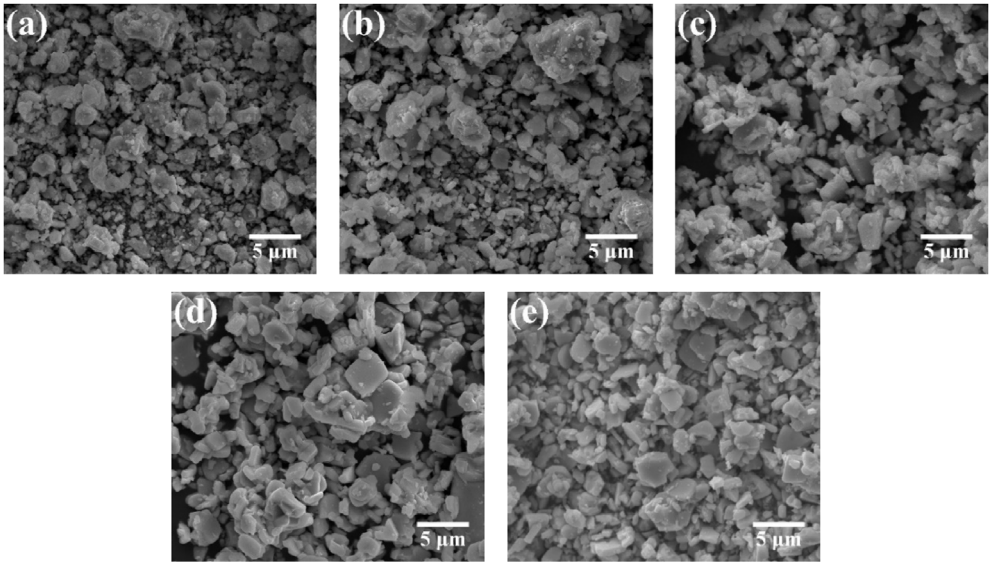

Fig. 2. SEM images of $Pb_{0.4}Bi_{2.1}La_{0.5}Nb_{1.7}Mn_{0.3}O_9$ samples: **(a)** PBLNM0, **(b)** PBLNM3, **(c)** PBLNM5, **(d)** PBLNM7, **(e)** PBLNM9.

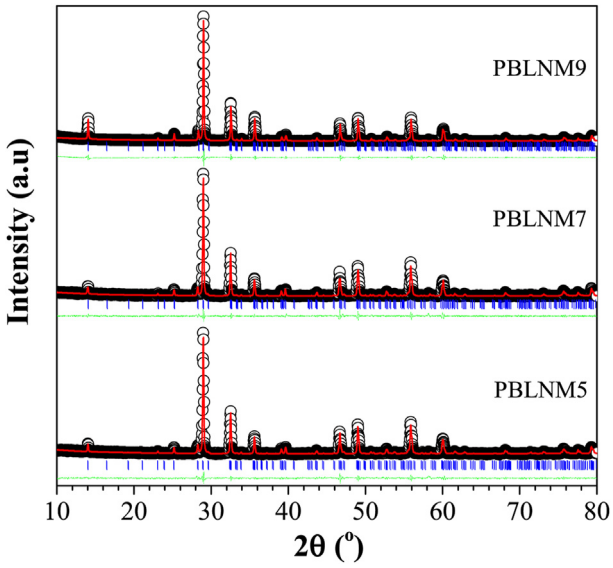

Fig. 3. Le Bail fits to XRD data for single-phase $Pb_{0.4}Bi_{2.1}La_{0.5}Nb_{1.7}Mn_{0.3}O_9$ samples: measured data (circles), fitted profile (red line), and difference profile (green line). The blue tick-marks indicate the positions of allowed Bragg reflections in the space group $A2_1am$. (For interpretation of the references to colour in this figure legend, the reader is referred to the Web version of this article.)

Table 1
Structural parameters of single-phase $Pb_{0.4}Bi_{2.1}La_{0.5}Nb_{1.7}Mn_{0.3}O_9$ obtained from XRD fits.

Parameter	PBLNM5	PBLNM7	PBLNM9
Space Group	$A2_1am$	$A2_1am$	$A2_1am$
Crystal class	Orthorhombic	Orthorhombic	Orthorhombic
a (Å)	5.5173(7)	5.5190(4)	5.5166(0)
b (Å)	5.4911(9)	5.4904(3)	5.4899(3)
c (Å)	25.1909(8)	25.1576(8)	25.1265(3)
V (Å^3)	763.210(3)	762.327(2)	760.977(3)
Z	4	4	4
R_p (%)	2.979	3.219	3.687
R_{wp} (%)	3.901	4.225	4.46
χ^2	1.439	1.560	1.591

Mn^{4+} ions; the ionic radius in six-fold coordination of Mn^{4+} (0.54 Å) is smaller than that of Mn^{3+} (0.645 Å) [23]. The mixed-valent Mn^{3+}/Mn^{4+} state could also be expected to give rise to ferromagnetic ordering via Mn^{3+}-O-Mn^{4+} double-exchange interactions [24], as discussed further below.

Fig. 4a shows the frequency dependence of the dielectric constant (ϵ) and dielectric loss (tan δ) of the single-phase products at room temperature. The dielectric constant decreases up to 100 kHz and then remains stable with further increasing frequency, which is typical behavior in ferroelectric materials. In the low-frequency range, the higher dielectric constant and dielectric loss arise from extrinsic factors, such as the presence of electronic, ionic, dipolar, and space-charge polarization; this is also caused by the Maxwell-Wagner effect, where charge carriers accumulate at the surface and at grain boundaries. The decrease of dielectric constant at high frequencies is because partial polarization mechanisms cannot follow the electric field, such that the main contribution to the dielectric constant is from electronic polarization and ionic polarization.

Fig. 4b shows the temperature dependence of the dielectric constant (ϵ) and dielectric loss (tan δ) of the single-phase products at 1 MHz, which best reflect the intrinsic factors. All samples show a single peak in the dielectric constant at 365 °C, corresponding to the ferroelectric-paraelectric phase transition (T_c). The well-defined peak at T_c indicates the predominance of ferroelectric properties according to $A2_1am$ symmetry in all samples. Compared with the parent compound $PbBi_2Nb_2O_9$ for which T_c = 557 °C [5], the T_c of $Pb_{0.4}Bi_{2.1}La_{0.5}Nb_{1.7}Mn_{0.3}O_9$ is significantly decreased. This is because the substitution of La^{3+} on the A-site, which does not have a lone pair, reduces the degree of BO_6 distortion. Furthermore, the broadness of the T_c peak for all samples indicates relaxor-ferroelectric behavior, unlike the parent compound. This behavior is attributed to the increased disorder of both the A-site cations (Pb/Bi/La) and B-site cations (Nb/Mn) in the structure, as previously reported using neutron diffraction analysis [18].

The magnitude of the dielectric constant initially increases from sample PBLNM5 to PBLMN7 and then decreases for PBLNM9, while the dielectric loss increases linearly with the increase in salt ratio, as shown in Fig. 4a-b. This can be explained by the increasing grain size, which allows the movement of domain walls to become easier and the sample to more readily become polarized, resulting in enhanced dielectric properties [17,25]. We also suggest that the trend in dielectric loss with salt ratio is a consequence of the increasing grain size, as listed in Table 2. Larger grains and hence a decrease in the number of grain boundaries allow the charge carriers to move more freely, contributing

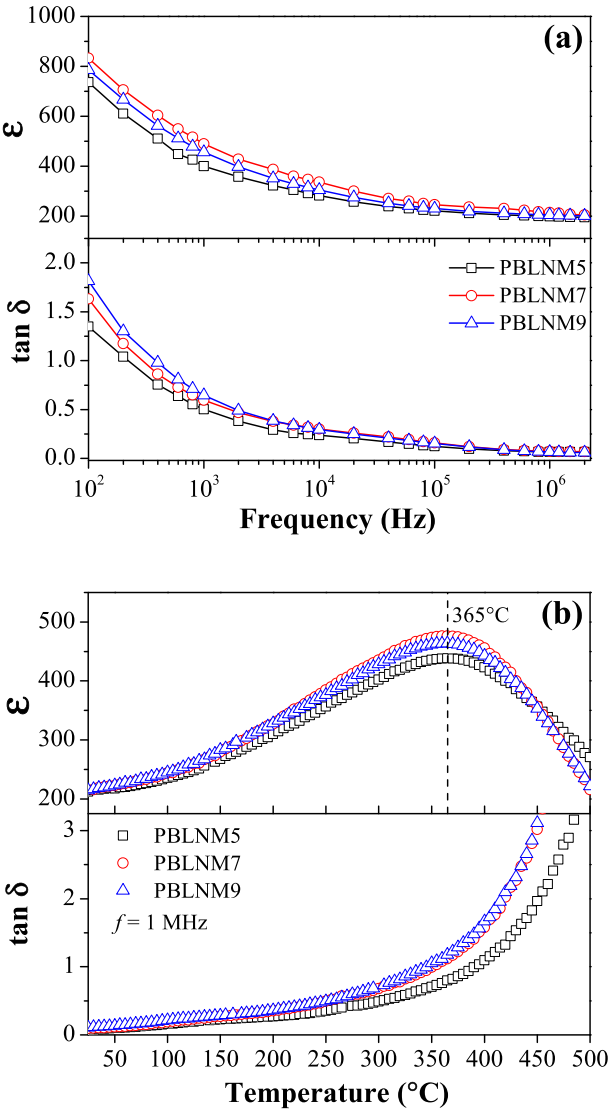

Fig. 4. (a) Dielectric constant (ϵ) and loss (tan δ) of single-phase $Pb_{0.4}Bi_{2.1}La_{0.5}Nb_{1.7}Mn_{0.3}O_9$ as a function of frequency at room temperature **(b)** Dielectric constant (ϵ) and loss (tan δ) of single-phase $Pb_{0.4}Bi_{2.1}La_{0.5}Nb_{1.7}Mn_{0.3}O_9$ as a function of temperature at 1 MHz.

Table 2
Variation of dielectric properties of single-phase samples of $Pb_{0.4}Bi_{2.1}La_{0.5}Nb_{1.7}Mn_{0.3}O_9$ measured at 1 MHz.

Sample	Grain size (μm)	T_c (°C)	ε_m	tan δ
PBLNM5	~1.8	365	438.39	0.801
PBLNM7	~2.3	365	476.14	1.079
PBLNM9	~2.4	365	463.47	1.179

to the increase in dielectric loss. These results may also be influenced by the hopping conduction of electrons associated with double exchange via Mn^{3+}-O-Mn^{4+} bonds. As explained above, samples prepared with a higher salt ratio show an increase in the proportion of Mn^{4+} ions.

In order to investigate the magnetic behavior of the $Pb_{0.4}Bi_{2.1}La_{0.5}Nb_{1.7}Mn_{0.3}O_9$ samples, the temperature dependence of the magnetic susceptibility (χ) was measured in zero-field-cooled (ZFC) mode on warming in an applied magnetic field of 1 T. Fig. 5a shows that the magnetic susceptibility smoothly decreases with increasing temperature and does not exhibit any anomalies, suggesting paramagnetic behavior. A Curie-Weiss fit to the linear region of the inverse

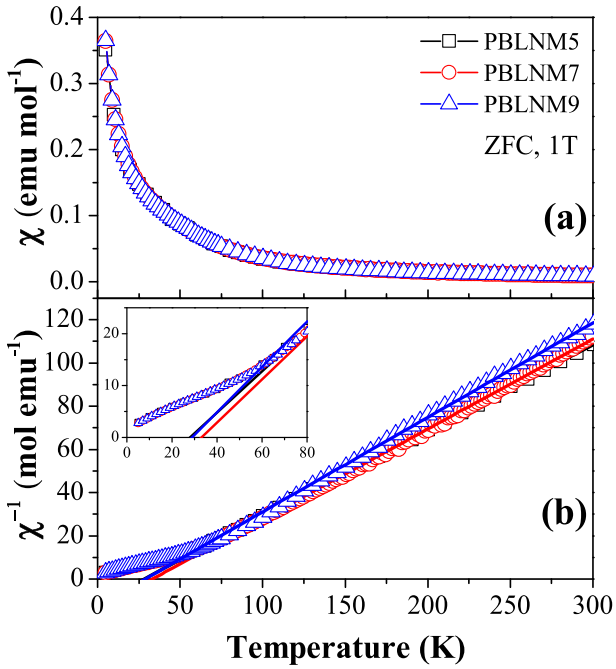

Fig. 5. (a) Magnetic susceptibility (χ) and **(b)** inverse magnetic susceptibility ($1/\chi$) of single-phase $Pb_{0.4}Bi_{2.1}La_{0.5}Nb_{1.7}Mn_{0.3}O_9$ measured from 5 to 300 K in an applied field of 1 T (after cooling in zero field). The straight lines are linear fits to the inverse susceptibility above 150 K using the Curie-Weiss law.

Table 3
Magnetic properties of single-phase samples of $Pb_{0.4}Bi_{2.1}La_{0.5}Nb_{1.7}Mn_{0.3}O_9$.

Sample	θ_{CW} (K)	μ_{eff} (μ_B)	M_s (emu g^{-1})	M_r (emu g^{-1})
PBLNM5	28.0	4.48	3.47	0.0069
PBLNM7	33.4	4.38	3.48	0.0103
PBLNM9	28.9	4.27	3.48	0.0087

susceptibility above 150 K was performed, as shown in Fig. 5b. The extracted Curie-Weiss temperatures (θ_{CW}) are positive for all the single-phase samples, as observed in the inset of Fig. 5b and listed in Table 3, indicating the predominance of ferromagnetic interactions. The largest θ_{CW} value of 33.4 K is found for sample PBLNM7, implying the most pronounced ferromagnetic interactions.

The spin-only effective moments (μ_{eff}) of Mn for the single-phase samples extracted from the Curie-Weiss fitting are listed in Table 3. The values lie between those expected for Mn^{3+} (~4.9 μ_B) and Mn^{4+} (~3.87 μ_B) [26,27]. Thus, all samples contain a mixture of both cations. The decrease in μ_{eff} with increasing oxide to salt ratio confirms that the proportion of Mn^{4+} increases, in agreement with the trend in the *c*-lattice parameter. The PBLNM5 sample contains more Mn^{3+} than Mn^{4+} (60% to 40%), PBLNM7 contains approximately equal proportions of Mn^{3+} and Mn^{4+}, and PBLNM9 contains less Mn^{3+} than Mn^{4+} (39% to 61%).

The tendency of more Mn^{4+} to be stabilized at higher salt ratios might be due to an oxide ion donor mechanism involving oxobasic SO_4^{2-} anions, according to Lux-Flood acid-base theory. It has been reported that molten salt fluxes tend to be oxidizing in solution, leading to products with higher oxidation states [28]. This might be further promoted by the oxygen-rich sintering atmosphere used in the present work. The oxidation of Mn^{3+} in Aurivillius compounds synthesized using the molten salt method has also been observed previously [8]. We note that a varying ratio of Mn^{3+}/Mn^{4+} would require a varying concentration of vacancies on other cation sites to achieve charge balance, an aspect that requires further study.

Mixed-valent Mn^{3+}/Mn^{4+} will enable double-exchange to take

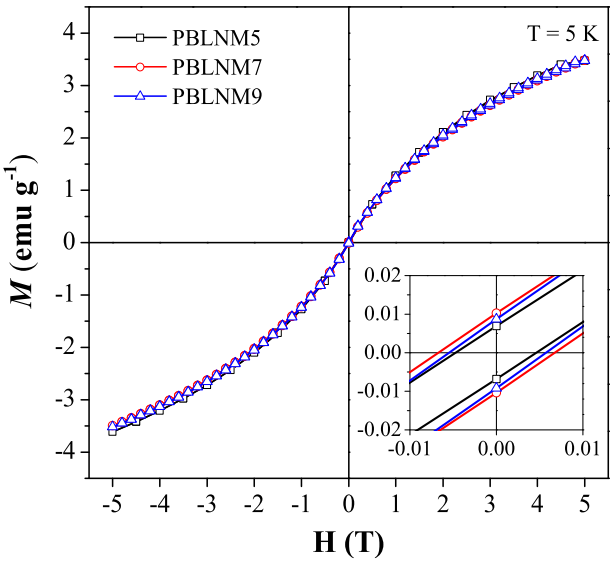

Fig. 6. Magnetization versus applied field for $Pb_{0.4}Bi_{2.1}La_{0.5}Nb_{1.7}Mn_{0.3}O_9$ measured at 5 K.

place, accounting for the ferromagnetic interactions observed in all the samples. However, the presence of double-exchange implies that clusters of linked MnO_6 octahedra exist in the structure, as previously suggested by the Raman mode observed at ~756 cm^{-1} [17]. The equal proportion of Mn^{3+} and Mn^{4+} in the PBLNM7 sample likely results in the highest probability of double-exchange interactions occurring within Mn-rich clusters, as suggested by the highest θ_{CW}. For PBLNM5 and PBLNM9, the higher proportion of either Mn^{3+} or Mn^{4+} will likely favor the antiferromagnetic super-exchange interactions Mn^{3+}-O-Mn^{3+} or Mn^{4+}-O-Mn^{4+}, leading to a decrease of θ_{CW}. It has commonly been observed that ferromagnetic behavior can be enhanced by combining mixed-valent magnetic cations in an equal ratio [29,30]. However, no ferromagnetic-paramagnetic transition peak (T_c) is observed in Fig. 5a because the total Mn-content is far below the percolation threshold for long-range magnetic ordering.

In order to verify the existence of ferromagnetic interactions, the magnetic field dependence of the magnetization was measured at a temperature of 5 K, as shown in Fig. 6. The magnetization increases with magnetic field in non-linear fashion and remains unsaturated in magnetic fields up to 5 T. A narrow hysteresis loop can be observed in the inset of Fig. 6, providing evidence for ferromagnetic properties. The remnant magnetization (M_r) is highest in the PBLNM7 sample (Table 3) and is consistent with an increased probability of double-exchange interactions as discussed above.

4. Conclusions

The double-layer Aurivillius compound $Pb_{0.4}Bi_{2.1}La_{0.5}Nb_{1.7}Mn_{0.3}O_9$ has been synthesized by a molten salt method using varying proportions of K_2SO_4/Na_2SO_4 flux. Single-phase products are obtained for oxide to salt ratios of 1:5 and higher. As the salt ratio increases, the unit cell volume decreases and the grains become larger with less agglomeration. The best dielectric properties are obtained for a salt ratio of 1:7, which at 1 MHz gives a ferroelectric transition temperature of 365 °C, a maximum dielectric constant of 476.14, and a dielectric loss (tan δ) of 1.079. Magnetic susceptibility measurements demonstrate the presence of mixed-valent Mn^{3+}/Mn^{4+}, where the tendency to stabilize Mn^{4+} increases with the salt ratio. The most pronounced ferromagnetic properties are obtained for a salt ratio of 1:7, as evidenced by the highest θ_{CW} and M_r. In conclusion, the Aurivillius compound $Pb_{0.4}Bi_{2.1}La_{0.5}Nb_{1.7}Mn_{0.3}O_9$ exhibits multiferroic properties, which are optimal when synthesized using a molar oxide to salt ratio of 1:7.

Declaration of competing interest

The authors declare that they have no known competing financial interests or personal relationships that could have appeared to influence the work reported in this paper.

Acknowledgments

This work was supported by the Ministry of Research, Technology and Higher Education (RISTEKDIKTI) of the Republic of Indonesia through the PMDSU Scholarship [Grant number 050/SP2H/LT/DRPM/2018]; and by the PKPI-PMDSU Scholarship [Grant number 1406.29/D3/PG/2018]with the University of Groningen, The Netherlands.

References

[1] J.F.Scott, Ferroelectric Memories, first ed., Springer-Verlag Berlin Heidelberg, New York, n.d. doi:10.1007/978-3-662-04307-3.
[2] W. Eerenstein, N.D. Mathur, J.F. Scott, Multiferroic and magnetoelectric materials, Nature 442 (2006) 759–765, https://doi.org/10.1016/j.actamat.2011.12.024.
[3] B. Aurivillius, Mixed bismuth oxides with layer lattices 1. The structure type of $CaNb_2Bi_2O_9$, Ark. För Kemi. 1 (1949) 463–480.
[4] E.C. Subbarao, A family of ferroelectric bismuth compounds, J. Phys. Chem. Solid. 23 (1962) 665–676, https://doi.org/10.1016/0022-3697(62)90526-7.
[5] H. Du, Y. Li, H. Li, X. Shi, C. Liu, Relaxor behavior of bismuth layer-structured ferroelectric ceramic with m = 2, Solid State Commun. 148 (2008) 357–360, https://doi.org/10.1016/j.ssc.2008.05.017.
[6] Ismunandar, B.A. Hunter, B.J. Kennedy, Cation disorder in the ferroelectric Aurivillius phase $PbBi_2Nb_2O_9$: an anamolous dispersion X-ray diffraction study, Solid State Ionics 112 (1998) 281–289, https://doi.org/10.1016/S0167-2738(98)00222-7.
[7] A.J.C. Buurma, G.R. Blake, T.T.M. Palstra, Multiferroic Materials : Physics and Properties, Elsevier Ltd., 2016, https://doi.org/10.1016/B978-0-12-803581-8.09245-6.
[8] Zulhadjri, B. Prijamboedi, A.A. Nugroho, N. Mufti, A. Fajar, T.T.M. Palstra, Ismunandar, Aurivillius phases of $PbBi_4Ti_4O_{15}$ doped with Mn^{3+} synthesized by molten salt technique: structure, dielectric, and magnetic properties, J. Solid State Chem. 184 (2011) 1318–1323, https://doi.org/10.1016/j.jssc.2011.03.044.
[9] P. Fang, P. Liu, Z. Xi, W. Long, X. Li, Structure and electrical properties of new Aurivillius oxides $(K_{0.16}Na_{0.84})_{0.5}Bi_{4.5}Ti_4O_{15}$ with manganese modification, J. Alloys Compd. 595 (2014) 148–152, https://doi.org/10.1016/j.jallcom.2014.01.152.
[10] A. Khokhar, P.K. Goyal, O.P. Thakur, A.K. Shukla, K. Sreenivas, Influence of lanthanum distribution on dielectric and ferroelectric properties of $BaBi_{4-x}La_xTi_4O_{15}$ ceramics, Mater. Chem. Phys. 152 (2015) 13–25, https://doi.org/10.1016/j.matchemphys.2014.11.074.
[11] S. Liu, S. Yan, H. Luo, L. Yao, Z. Hu, S. Huang, L. Deng, Enhanced magnetoelectric coupling in La-modified $Bi_5Co_{0.5}Fe_{0.5}Ti_3O_{15}$ multiferroic ceramics, J. Mater. Sci. 53 (2018) 1014–1023, https://doi.org/10.1007/s10853-017-1604-6.
[12] B. Prijamboedi, Zulhadjri, A.A. Nugroho, Ismunandar, Synthesis and structure analysis of Aurivillius phases $Pb_{1-x}Bi_{4+x}Ti_{4-x}Mn_xO_{15}$, J. Chin. Chem. Soc. 56 (2009) 1108–1111, https://doi.org/10.1002/jccs.200900160.
[13] J. Xiao, H. Zhang, Y. Xue, Z. Lu, X. Chen, P. Su, F. Yang, X. Zeng, The influence of Ni-doping concentration on multiferroic behaviors in $Bi_4NdTi_3FeO_{15}$ ceramics, Ceram. Int. 41 (2015) 1087–1092, https://doi.org/10.1016/j.ceramint.2014.09.033.
[14] M. García-guaderrama, G. Guadalupe, C. Arizaga, A. Durán, Effect of synthesis conditions on the morphology and crystal structure, Ceram. Int. 40 (2014) 7459–7465, https://doi.org/10.1016/j.ceramint.2013.12.094.
[15] X. Chen, Z. Lu, F. Huang, J. Min, J. Li, J. Xiao, F. Yang, X. Zeng, Molten salt synthesis and magnetic anisotropy of multiferroic $Bi_4NdTi_3Fe_{0.7}Ni_{0.3}O_{15}$ ceramics, J. Alloys Compd. 693 (2017) 448–453, https://doi.org/10.1016/j.jallcom.2016.09.214.
[16] D.G. Porob, P.A. Maggard, Synthesis of textured $Bi_5Ti_3FeO_{15}$ and $LaBi_4Ti_3FeO_{15}$ ferroelectric layered Aurivillius phases by molten-salt flux methods, Mater. Res. Bull. 41 (2006) 1513–1519, https://doi.org/10.1016/j.materresbull.2006.01.020.
[17] T.P. Wendari, S. Arief, N. Mufti, V. Suendo, A. Prasetyo, Ismunandar, J. Baas, G.R. Blake, Synthesis Zulhadjri, Structural analysis and dielectric properties of the double-layer Aurivillius compound $Pb_{1-2x}Bi_{1.5+2x}La_{0.5}Nb_{2-x}Mn_xO_9$, Ceram. Int. 45 (2019) 17276–17282, https://doi.org/10.1016/j.ceramint.2019.05.285.
[18] T.P. Wendari, S. Arief, N. Mufti, A. Insani, J. Baas, G.R. Blake, Zulhadjri, Structural and multiferroic properties in double-layer Aurivillius phase $Pb_{0.4}Bi_{2.1}La_{0.5}Nb_{1.7}Mn_{0.3}O_9$ prepared by molten salt method, J. Alloys Compd. 820 (2020) 153145, https://doi.org/10.1016/j.jallcom.2019.153145.
[19] C. Lu, C. Wu, Preparation, sintering, and ferroelectric properties of layer-structured strontium bismuth titanium oxide ceramics, J. Eur. Ceram. Soc. 22 (2002) 707–714, https://doi.org/10.1016/S0955-2219(01)00377-6.
[20] X. Tian, F. Gao, S. Qu, H. Ma, B. Wang, Effects of molten salt content and reaction temperature on molten salt preparation of $CaNaBi_2Nb_3O_{12}$ powder, J. Mater. Sci. Mater. Electron. 26 (2015) 6189–6193, https://doi.org/10.1007/s10854-015-3201-2.

[21] Z. Zhao, X. Li, H. Ji, M. Deng, Formation mechanism of plate-like $Bi_4Ti_3O_{12}$ particles in molten salt fluxes, Integrated Ferroelectrics 154 (2014) 154–158, https://doi.org/10.1080/10584587.2014.904705.
[22] K. Miura, Electronic properties of ferroelectric $SrBi_2Ta_2O_9$, $SrBi_2Nb_2O_9$, and $PbBi_2Nb_2O_9$ with optimized structures, Appl. Phys. Lett. 80 (2002) 2967–2969, https://doi.org/10.1063/1.1474607.
[23] R.D. Shannon, Revised effective ionic radii and systematic studies of interatomie distances in halides and chaleogenides, Acta Crystallogr. 32 (1976) 751–767.
[24] B. Zhang, C. Cao, G. Li, F. Li, W. Ji, S. Zhang, M. Ren, H. Zhang, R.Q. Zhang, Z. Zhong, Z. Yuan, S. Yuan, G.R. Blake, 2p-insulator heterointerfaces: creation of half-metallicity and anionogenic ferromagnetism via double exchange, Phys. Rev. B 97 (2018) 165109, https://doi.org/10.1103/PhysRevB.97.165109.
[25] X. Tian, S. Qu, H. Ma, Z. Pei, B. Wang, Effect of grain size on dielectric and piezoelectric properties of bismuth layer structure $CaBi_2Nb_2O_9$ ceramics, J. Mater. Sci. Mater. Electron. 27 (2016) 13309–13313, https://doi.org/10.1007/s10854-016-5480-7.
[26] C.A. López, M.E. Saleta, J.C. Pedregosa, R.D. Sánchez, J.A. Alonso, M.T. Fernández-díaz, Cationic disorder and Mn^{3+}/Mn^{4+} charge ordering in the B' and B'' sites of $Ca_3Mn_2NbO_9$ perovskite: a comparison with $Ca_3Mn_2WO_9$, J. Solid State Chem. 210 (2014) 1–9, https://doi.org/10.1016/j.jssc.2013.10.039.
[27] K. Nakade, K. Hirota, M. Kato, H. Taguchi, Effect of the Mn^{3+} ion on electrical and magnetic properties of orthorhombic perovskite-type $Ca(Mn_{1-x}Ti_x)O_{3-\delta}$, Mater. Res. Bull. 42 (2007) 1069–1076, https://doi.org/10.1016/j.materresbull.2006.09.013.
[28] J. Boltersdorf, N. King, P.A. Maggard, Flux-mediated crystal growth of metal oxides: synthetic tunability of particle morphologies, sizes, and surface features for photocatalysis research, CrystEngComm 17 (2015) 2225–2241, https://doi.org/10.1039/c4ce01587h.
[29] C.X. Chen, Y.K. Liu, R.K. Zheng, Magnetic and ferroelectric properties of $SmBi_4Fe_{0.5}Co_{0.5}Ti_3O_{15}$ compounds prepared with different synthesis methods, J. Mater. Sci. Mater. Electron. 28 (2017) 7562–7567, https://doi.org/10.1007/s10854-017-6446-0.
[30] Y. Wu, T. Yao, Y. Lu, B. Zou, X. Mao, F. Huang, H. Sun, X. Chen, Magnetic, dielectric, and magnetodielectric properties of Bi-layered perovskite $Bi_{4.25}Gd_{0.75}Fe_{0.5}Co_{0.5}Ti_3O_{15}$, J. Mater. Sci. 52 (2017) 7360–7368, https://doi.org/10.1007/s10853-017-0971-3.